Soft Robotics

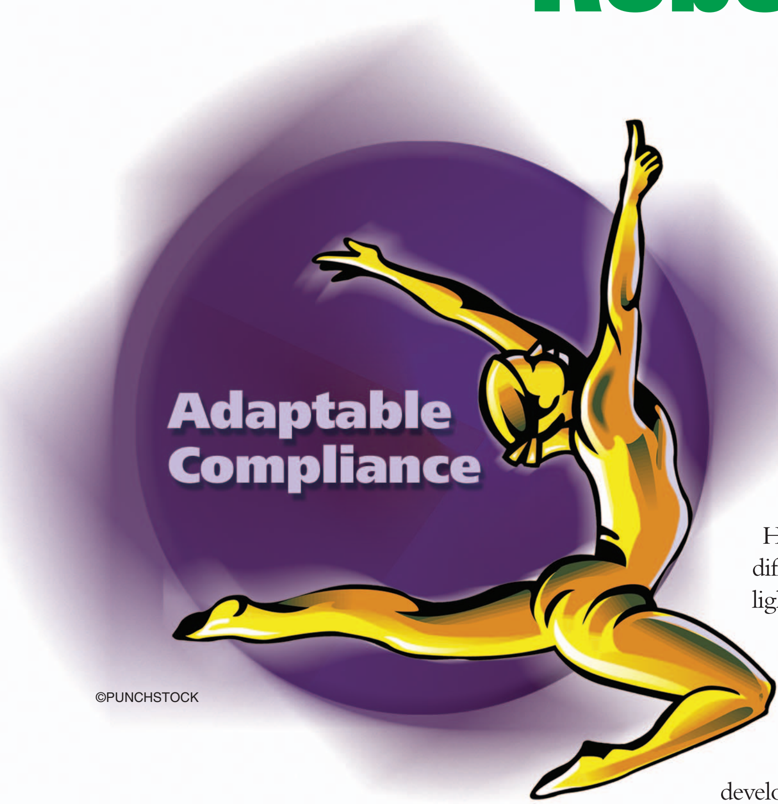

©PUNCHSTOCK

From Torque Feedback-Controlled Lightweight Robots to Intrinsically Compliant Systems

BY ALIN ALBU-SCHÄFFER, OLIVER EIBERGER, MARKUS GREBENSTEIN, SAMI HADDADIN, CHRISTIAN OTT, THOMAS WIMBÖCK, SEBASTIAN WOLF, AND GERD HIRZINGER

After decades of intensive research, it seems that we are getting closer to the time when robots will finally leave the cages of industrial robotic workcells and start working in the vicinity of and together with humans. This opinion is not only shared by many robotics researchers but also by the leading automotive and IT companies and, of course, by some clear-sighted industrial robot manufacturers. Several technologies required for this new kind of robots reached the necessary level of performance, e.g., computing power, communication technologies, sensors, and electronics integration. However, it is clear that these human-friendly robots will look very different than today's industrial robots. Rich sensory information, lightweight design, and soft-robotic features are required to reach the expected performance and safety during interaction with humans or in unknown environments. In this article, we will present and compare two approaches for reaching the aforementioned soft-robotic features. The first one is the mature technology of torque-controlled lightweight robots (LWRs) developed during the past decade at the German Aerospace Center (DLR) (arms, hands, a humanoid upper body, and a crawler). Several products resulted from this research and are currently being commercialized through cooperations with different industrial partners (DLR-KUKA LWR, DLR-HIT-Schunk hand, DLR-Brainlab medical robot). The second technology, still a topic of worldwide ongoing research, is variable compliance actuation that implements the soft-robotic features mainly in hardware.

We start by reviewing the main design and control ideas of actively controlled compliant systems using the DLR arms, hands, and the humanoid manipulator Justin as examples. We take these robots as a performance reference, which we are currently trying to outperform with new variable stiffness actuators. This leads us to the motivation of the variable stiffness actuator design. We present the main design ideas and our first results with the new actuator prototypes. Some experimental examples providing first validation of the performance and safety gain of this design approach are presented finally.

Mechatronic Design of LWR with Joint Torque Sensing

In this section, a mechatronic design approach for obtaining the robots with the desired lightweight and performance properties is briefly described. The following aspects are of particular relevance.

- *Lightweight structures*: lightweight metals or composite materials are used for the robot links.
- *High-energy motors*: In contrast to industrial robots, motors with high torque at moderate speed, low energy loss, and fast dynamic response are of interest rather than high-velocity motors. For this purpose, special motors, namely, the DLR Robodrive, have been designed.
- *Gearing with high load to weight ratio*: Harmonic drive gears are used for the DLR robots.

Digital Object Identifier 10.1109/MRA.2008.927979

1070-9932/08/$25.00©2008 IEEE

- *Integration of electronics into the joint, leading to a modular design*: This allows the design of robots of increasing kinematic complexity based on integrated joints as in the case of the DLR humanoid Justin. Moreover, one obtains a self-contained system, which is well suited for autonomous, mobile applications.
- *Full-state measurement in the joints*: As will be outlined in the "Compliance Control for Lightweight Arms" section, our robots use torque sensing in addition to position sensing to implement a compliant behavior and a smooth, vibration-free motion. The full-state measurement in all joints is performed at 3-kHz cycle using strain-gauge-based torque-sensors, motor position sensing based on magnetoresistive encoders, and link side position sensors based on potentiometers (used only as additional sensors for safety considerations).
- *Sensor redundancy for safety*: Positions, forces, and torques are redundantly measured.

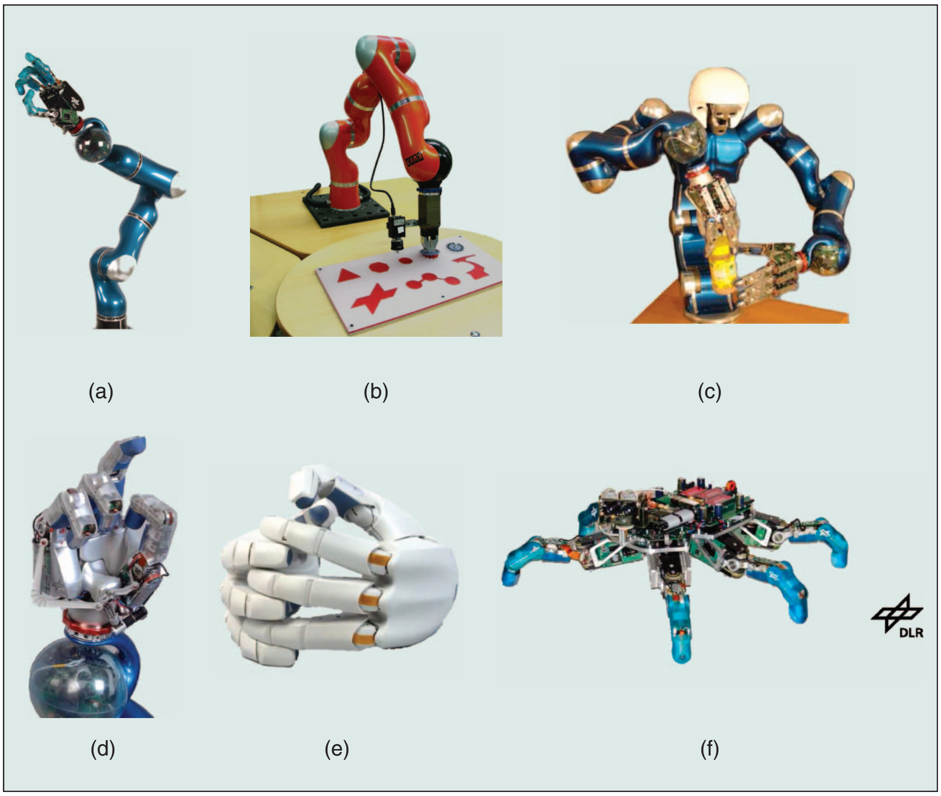

Figure 1. *Overview of the DLR Robots. (a) The DLR-LWR-III equipped with the DLR-Hand-II. (b) The DLR-KUKA-LWR-III that is based on the DLR-LWR-III. (c) The DLR humanoid manipulator Justin. (d) The DLR-Hand-II-b, a redesign of the DLR-Hand-II. (e) The DLR-HIT hand, a commercialized version of the DLR-Hand-II. (f) The DLR-Crawler, a walking robot based on the fingers of the DLR-Hand-II.*

These basic design ideas are used for the joints in the arms, hands, and torso of the upper body system Justin (Figure 1). Moreover, because the joints are self-contained, it is straightforward to combine these modules to obtain different kinematic configurations. For example, the fingers have been used to build up a crawler prototype. Figure 2 shows the exploded view of one LWR-III (DLR-LWR-III) joint.

Compliance Control for Lightweight Arms

In the next two sections, the framework used to implement active compliance control based on joint torque sensing is summarized. The lightweight design is obtained by using relatively high gear reduction ratios (typically 1:100 or 1:160), leading to joints that are hardly backdrivable and have already moderate intrinsic compliance. Therefore, we model the robot as a flexible joint system. Thus, measuring the torque after the gears is essential for implementing high-performance soft-robotic features. When implementing compliant control laws, the torque signal is used both for reducing the effects of joint friction and for damping the vibrations related to the joint compliance. Motor position feedback is used to impose the desired compliant behavior. The control framework is constructed from a passivity control perspective by giving a simple and intuitive physical interpretation in terms of energy shaping to the feedback of the different state vector components.

- A physical interpretation of the joint torque feedback loop is given as the shaping of the motor inertia.
- The feedback of the motor position can be regarded as shaping of the potential energy.

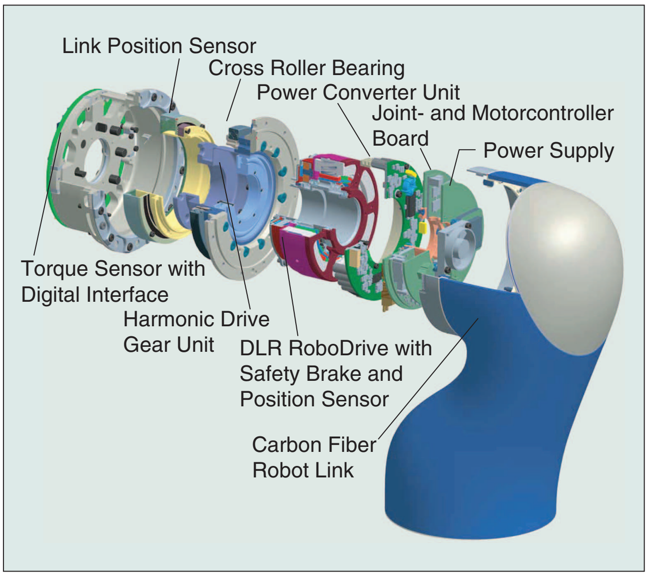

Figure 2. *The mechatronic joint design of the DLR-LWR-III, including actuation, electronics, and sensing.*

Joint Torque Control: Shaping the Actuator Kinetic Energy

To simplify the analysis and to be able to generalize the joint level approach also to Cartesian coordinates, the idea of interpreting the joint torque feedback as the shaping of the motor inertia plays a central role [1], [2]. It enables one to directly use the torque feedback within the passivity framework and conceptually divides the controller design into two steps. One is related to the torque feedback and the other to the position feedback (Figure 3). As sketched in the figure and presented in detail in [1] and [2], the torque control feedback reduces the motor inertia to a value $\boldsymbol{B}_\theta$, lower than the real value $\boldsymbol{B}$. (Although friction is not depicted in Figure 3, note that the frictional effect will be reduced by the same factor $\boldsymbol{B}_\theta^{-1}\boldsymbol{B}$.)

Motor Position-Based Feedback: Shaping the Potential Energy

Using motor position $\boldsymbol{\theta}$ for control, and not the link position $\boldsymbol{q}$, is essential for the passivity properties of the controller. However, the desired position and stiffness are usually formulated in terms of the link position. For the impedance controllers of the DLR LWRs, the position feedback has the form

$$\boldsymbol{u} = -\frac{\partial V_P(\bar{\boldsymbol{q}}(\boldsymbol{\theta}))}{\partial \boldsymbol{\theta}} - \boldsymbol{D}_\theta \dot{\boldsymbol{\theta}} + \boldsymbol{g}(\bar{\boldsymbol{q}}(\boldsymbol{\theta})), \qquad (1)$$

with $\boldsymbol{u}$ being the input to the torque controller, V_P a positive definite potential function, and $\boldsymbol{D}_\theta$ a positive definite damping matrix chosen for a well-damped transient behavior [3]. This is the classical structure of a compliance controller for rigid robots, except for the fact that, instead of the link position $\boldsymbol{q}$, a position signal $\bar{\boldsymbol{q}}(\boldsymbol{\theta})$ is used, which is statically equivalent to $\boldsymbol{q}$, i.e., $\bar{\boldsymbol{q}}(\boldsymbol{\theta}) = \boldsymbol{q}$ if $\dot{\boldsymbol{q}} = \dot{\boldsymbol{\theta}} = \boldsymbol{0}$ and can be computed numerically [1], [2]. (In practice, we often use the trivial approximation $\bar{\boldsymbol{q}}(\boldsymbol{\theta}) = \boldsymbol{\theta}$ for applications in which high position accuracy is not required.)

Because now the position feedback is again only a function of $\boldsymbol{\theta}$, the passivity of the controlled robot is given with respect to the input-output pair $(\boldsymbol{\tau}_{\text{ext}}, \dot{\boldsymbol{q}})$ (Figure 3).

To obtain a joint level impedance controller, one can simply use $V_P(\bar{\boldsymbol{q}}) = \frac{1}{2}(\boldsymbol{q}_d - \bar{\boldsymbol{q}})^T K_J (\boldsymbol{q}_d - \bar{\boldsymbol{q}})$, whereas for Cartesian impedance control, V_P is defined as a function of the Cartesian coordinates $\boldsymbol{x}(\bar{\boldsymbol{q}})$, as detailed in the following section. The external torque $\boldsymbol{\tau}_{\text{ext}}$ is then replaced by the external force $\boldsymbol{F}_{\text{ext}}$. (The relation between the external tip force $\boldsymbol{F}_{\text{ext}}$ and the external joint torque $\boldsymbol{\tau}_{\text{ext}}$ is $\boldsymbol{\tau}_{\text{ext}} = \boldsymbol{J}(\boldsymbol{q})^T \boldsymbol{F}_{\text{ext}}$.) A Lyapunov function for the system is obtained by summing the kinetic and the gravity-potential energy of the rigid part of the robot dynamics with the kinetic energy of the scaled motor inertia and the potential energy of the controller [1], [2].

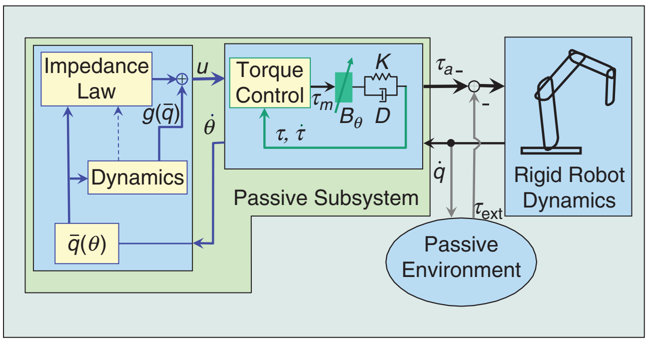

Figure 3. *Representation of the compliance-controlled robot as a connection of passive blocks.* $\boldsymbol{\theta}$ *is the motor position, and* q *the link position.* B, K, *and* D *are the motor inertia, joint stiffness, and damping matrices, respectively.* τ *is the elastic joint torque,* τ_a *the total (elastic and damping) joint torque,* τ_{ext} *the external torque, and* g *the gravity torque.*

Impedance Control for Complex Kinematic Chains

In this section, we show how to apply the impedance control concept from the previous section to kinematically more complex robot systems, like artificial hands and anthropomorphic two-handed manipulator systems.

The design of appropriate potential functions $V_P(\bar{\boldsymbol{q}})$ is discussed in this section. Furthermore, we will assume the potential function V_s of a virtual spatial spring, e.g., the ones designed in [4]–[6], as a basic building block. This potential function $V_s(\boldsymbol{H}_1, \boldsymbol{H}_2, \mathcal{K})$ depends on two frames $\boldsymbol{H}_1 \in SE(3)$ and $\boldsymbol{H}_2 \in SE(3)$, between which the spring is acting, and also on some configuration-independent internal parameters $\mathcal{K}$, like the stiffness values or the rest length.

Artificial Hands

Similar to the DLR lightweight arm, the DLR-Hand-II is equipped with joint torque sensors in addition to joint position measurements. Therefore, it is possible to apply the impedance control aspects as presented in the previous section to our anthropomorphic robot hand. The feedback of the torque sensors is used to increase the backdrivability, respectively the sensitivity, of the joints. Because of the small link masses and the high mechanical joint stiffness, vibration damping is not an issue here. Therefore, the approximation $\boldsymbol{q} = \boldsymbol{\theta} = \bar{\boldsymbol{q}}$ can be made. While joint and Cartesian impedance control are used for power grasp and independent fingertip motion, respectively, the most interesting case from a control point of view is the fine manipulation of a grasped object as all degrees of freedom (DoF) of the hand can contribute to its motion. In this case, the combined system containing arm, hand, and object represents a parallel robot (Figure 4). The task coordinates consist of two contributions. On the one hand, the Cartesian coordinates of the grasped object and, on the other hand, the coordinates that are related to internal forces.

In [7], we introduced a passivity-based object-level controller for a multifingered hand based on a virtual object similar to [8]. In contrast to the intrinsically passive controller (IPC) [8], the object frame is defined uniquely by the $i = 1 \ldots N$ Cartesian fingertip positions $\boldsymbol{p}_i(\bar{\boldsymbol{q}})$ by an appropriate kinematic relationship. The definition is such that it enables the spanning of the null space of the grasp matrix by internal forces generated by virtual elastic elements connecting the virtual object frame with the fingertips (Figure 4).

The definition of a potential function $V_P(\bar{\boldsymbol{q}})$ to derive at an object-level controller is then described by the superposition of two potentials: the potential of a spatial spring $V_s(\boldsymbol{H}_{ho}(\bar{\boldsymbol{q}}),$

$\boldsymbol{H}_{ho,d}, \mathcal{K}_{ho})$ between the virtual object frame $\boldsymbol{H}_{ho}(\bar{\boldsymbol{q}})$ and a virtual equilibrium frame $\boldsymbol{H}_{ho,d}$ and a potential $V_{hc}(\bar{\boldsymbol{q}}, \mathcal{K}_{hc})$ describing the ith spring connecting the virtual object with the ith frame of the fingertips $\boldsymbol{H}_{f,i}(\bar{\boldsymbol{q}})$ for $i = 1 \ldots N$ that are used to generate internal forces, i.e.,

$$V_P(\bar{\boldsymbol{q}}) = V_s(\boldsymbol{H}_{ho}(\bar{\boldsymbol{q}}), \boldsymbol{H}_{eq}, \mathcal{K}_{ho}) + V_{hc}(\bar{\boldsymbol{q}}, \mathcal{K}_{hc}). \tag{2}$$

The expressions $\mathcal{K}_{ho}$ and $\mathcal{K}_{hc}$ contain the stiffness matrix of the spatial spring and the coupling spring parameters, respectively. The potential for the coupling springs is different from the potentials for spatial springs and is chosen to be spherical for each fingertip i [7].

$$V_{hc}(\bar{\boldsymbol{q}}, \mathcal{K}_{hc}) = \frac{1}{2}\sum_{i=1}^{N} \mathcal{K}_{hc,i}[\|\Delta \boldsymbol{p}_i(\bar{\boldsymbol{q}})\| - \boldsymbol{l}_{i,d}]^2, \tag{3}$$

with $\Delta \boldsymbol{p}_i(\bar{\boldsymbol{q}}) = \boldsymbol{p}_i(\bar{\boldsymbol{q}}) - \boldsymbol{p}_{ho}(\bar{\boldsymbol{q}})$ being the distance from the position of the fingertip frame i to the virtual object frame position $\boldsymbol{p}_{ho}$, $l_{I,d}$ the desired rest length, and $K_{hc,i} > 0$ the corresponding coupling stiffness.

Employing Impedance Control for Two-Handed Manipulation

A natural extension of the impedance control approaches for the arms and hands allows one to formulate intuitive compliance behaviors also for more complex anthropomorphic manipulators like the humanoid manipulator Justin [Figure 1(c)]. This system was built at DLR as a test bed for studying two-handed manipulation tasks. It consists of two four-fingered artificial hands, two lightweight arms, and a sensor head mounted on a movable torso including the neck. Overall, Justin has 43 DoF.

Let us first consider the problem of controlling two arms. The end-effector frames of the right and left arm will be denoted as $\boldsymbol{H}_r(\bar{\boldsymbol{q}})$ and $\boldsymbol{H}_l(\bar{\boldsymbol{q}})$, respectively. Similar to multifingered hands, the compliance control of two arms has to handle the interaction forces between the two arms as well as the forces that the two arms exert cooperatively on the environment. The implementation, however, is even simpler in this case and can be done by combining two spatial springs. One spatial spring defines the relative compliance between the arms and can be described in a straightforward way by the potential function $V_s(\boldsymbol{H}_r(\bar{\boldsymbol{q}}), \boldsymbol{H}_l(\bar{\boldsymbol{q}}), \mathcal{K}_c)$. For implementing the cooperative action of the two arms, it is useful to rely on a virtual object frame $\boldsymbol{H}_o(\boldsymbol{H}_r(\bar{\boldsymbol{q}}), \boldsymbol{H}_l(\bar{\boldsymbol{q}}))$ depending on the two end-effector frames of the right and left arm. This object frame describes a relevant pose in between the arms (usually just the mean between the pose of the right and left arm) and thus represents the pose of a grasped object. This virtual object is then connected via a spatial spring $\mathcal{K}_o$ to a virtual equilibrium pose $\boldsymbol{H}_{o,d}$. In combination with the coupling stiffness, one can thus intuitively define an impedance behavior that is useful for grasping large objects with two arms. The resulting potential function is given by

$$\begin{aligned} V_P(\bar{\boldsymbol{q}}) = {} & V_s(\boldsymbol{H}_o(\boldsymbol{H}_r(\bar{\boldsymbol{q}}), \boldsymbol{H}_l(\bar{\boldsymbol{q}})), \boldsymbol{H}_{o,d}, \mathcal{K}_o) \\ & + V_s(\boldsymbol{H}_r(\bar{\boldsymbol{q}}), \boldsymbol{H}_l(\bar{\boldsymbol{q}}), \mathcal{K}_c). \end{aligned} \tag{4}$$

In case of a two-handed system, such a compliance behavior can easily be combined with the object-level compliance potentials designed for artificial hands. Therefore, the virtual viscoelastic springs are now attached to the virtual object frames $\boldsymbol{H}_{r,o}(\bar{\boldsymbol{q}})$ and $\boldsymbol{H}_{l,o}(\bar{\boldsymbol{q}})$ of the hands instead of attaching them directly to the end effectors of the arms (Figure 5). In combination with the interconnection potentials $V_{hcr}(\bar{\boldsymbol{q}}, \mathcal{K}_{hcr})$ and $V_{hcl}(\bar{\boldsymbol{q}}, \mathcal{K}_{hcl})$ for the right and left hand, the complete potential function is now given by

$$\begin{aligned} V_P(\bar{\boldsymbol{q}}) = {} & V_s(\boldsymbol{H}_o(\boldsymbol{H}_{r,o}(\bar{\boldsymbol{q}}), \boldsymbol{H}_{l,o}(\bar{\boldsymbol{q}})), \boldsymbol{H}_{o,d}, \mathcal{K}_o) \\ & + V_s(\boldsymbol{H}_{r,o}(\bar{\boldsymbol{q}}), \boldsymbol{H}_{l,o}(\bar{\boldsymbol{q}}), \mathcal{K}_c) \\ & + V_{hcr}(\bar{\boldsymbol{q}}, \mathcal{K}_{hcr}) + V_{hcl}(\bar{\boldsymbol{q}}, \mathcal{K}_{hcl}). \end{aligned} \tag{5}$$

Note that all spatial springs generate joint torques for the arms, hands, and torso by computing the total derivative of the potential function with respect to the generalized coordinates of the complete mechanism [c.f. (1)]. The presented control approach results in a passive closed-loop system by design, and it is therefore related to other intuitive passivity-based control approaches like the IPC

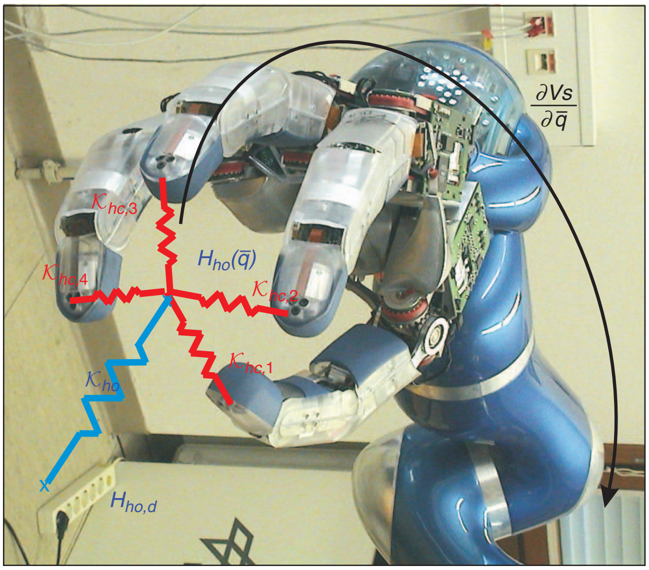

Figure 4. *DLR-Hand-II superimposed by the virtual springs defined by the potential functions in (2) and the virtual object.*

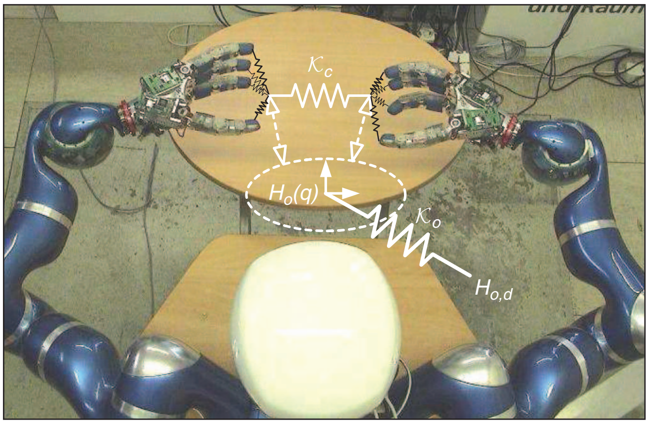

Figure 5. *Two-hand impedance behavior by combining the object-level impedances of the hands and the arms.*

[8]. Moreover, the chosen set of virtual spatial springs allows for a conceptually simple physical interpretation and consequently for an intuitive parametrization in any higher-level planning stage.

Adjusting the Mechanical Compliance: Motivation of the Variable Stiffness Actuator Design

From Actively Controlled to Passive Compliance

The paradigm of torque-controlled LWRs was presented in some detail up to now. Various robot examples and the underlying control concepts were introduced. On the basis of the experience gained with this successful approach, we were also trying to identify its limitations and recognize new directions of research for further increasing the performance and safety of robots.

The limitations of the achievable compliance by active control especially becomes an issue when considering the protection of the robot joint from external overload [9]–[11]. (This is due to the limited sensor precision, model accuracy, and sampling time as well as the motor saturation.) This threat can be diminished by deliberately introducing mechanical compliance into the joint. Furthermore, future robotic systems are supposed to execute tasks with similar speed and dexterity to humans. Extreme examples show that humans are capable of generating enormous joint speeds such as shoulder rotation of $6{,}900^\circ - 9{,}800^\circ/\mathrm{s}$ during a baseball pitch of a professional player [12]. This speed range is currently not realizable by robots if the torque range and the weight of the joint should also be compatible with human values. Therefore, new actuation concepts are sought for so as to approach such requirements. The concept of variable stiffness actuation (VSA), or its generalization of variable impedance actuation (VIA), seems to be a promising solution in this context, and its design and control was addressed in numerous publications [9], [13]–[16].

An elastic element in the joint serves as an energy storage mechanism, possibly decreasing the energy consumption of the entire system during the task execution, e.g., when playing drums or during running. Furthermore, the stored energy can be used to considerably increase the link speed as exemplified in the "Throwing" section. In contrast to the active compliance case, the robot remains compliant even in the case of deactivation or malfunction of the joint, thus potentially increasing the safety of humans interacting with the robot and protecting the robot joint from external impacts.

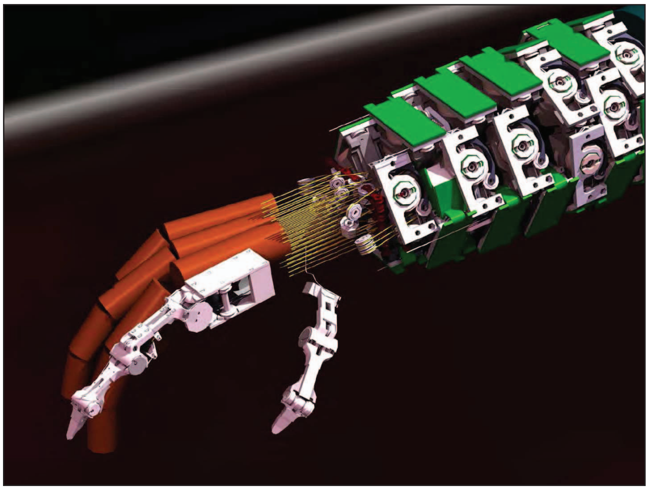

Figure 6. The integrated DLR hand-arm system.

Our goal is, based on our experience with torque-controlled LWRs, to built up a fully integrated VSA hand-arm system (Figure 6) for a close, safe, and performant interaction with humans while fulfilling the aforementioned requirements as close as possible.

Naturally, such a fundamental paradigm shift comes at a certain cost. The increased number of actuators and the small intrinsic damping are certainly some of the major challenges in controlling a variable compliance joint. (Introducing mechanical damping into the system would increase the open-loop performance at the cost of higher complexity, weight, and energy losses.) The expected reduction in absolute position accuracy because of the elasticity needs to be compensated for high precision tasks by external sensing, e.g., vision. Furthermore, a lower mechanical bandwidth will result from the generally lower joint stiffness. Regarding the realizable compliance, the first prototypes are expected to implement a diagonal joint stiffness matrix only. This is posing some limitations on the structure of the achievable Cartesian compliance [17]. However, if necessary, the couplings can still be obtained by active control as described in the "Compliance Control for Lightweight Arms" and "Impedance Control for Complex Kinematic Chains" sections.

To exemplify some possible advantages of the VSA design, a preliminary discussion of the influence of joint compliance on human and robot safety is presented before introducing the hardware design in the "New Hardware Design Concepts" section.

Protecting the Robot Joint and the Human by Variable Joint Stiffness

Rigid impacts at high speeds pose an enormous threat to the robot joint [11]. The exceedance of the maximum nominal joint torques is already shown at less than half of the maximum speed of the DLR-LWR-III. This problem necessitates fast collision detection and reaction schemes to prevent damage to the manipulator. (Results from [27] indicate that this is only possible up to a certain impact velocity that is far below the maximum velocity of the manipulator. Especially, the joint-torque sensor and the gears can be severely damaged.) In contrast, the VSA actuators limit in an intrinsic way the impact joint torques by elastically decoupling the link from gearbox and motor for the duration of the impact. To visualize this effect, a one-dimensional translational example (Figure 7) was simulated. In Figure 8, the joint force F_{Spring} during an impact with a human head at 2 m/s for a variable stiffness (VS) joint is depicted. One can see that it decreases dramatically for a joint stiffness reduced by one or two orders of magnitude compared with the DLR-LWR-III, thus substantially reducing the load of the joint. First experimental results confirming the aforementioned statements are shown in the "Experimental Validation of Joint Overload Protection" section.

The possible injury of the human during such rigid impacts is discussed in detail in [11] and [18]. It is shown there that the impact forces (which are mainly related to the impact velocity), and thus the potential injury of a human, do not depend on the joint stiffness already for link inertias and joint stiffness similar to the ones of the DLR-LWR-III. In Figure 8, the head injury criterion (HIC) and the impact forces F_{ext} are depicted, showing that even with reduced joint stiffness, they basically stay the same. This can be explained by the fact that rigid impacts are practically over before the joint force starts rising. In other words, it is only the link inertia involved in such hard and rigid impacts.

A case for which compliance of the robot does reduce the injury risk for humans is given by impacts with sharp tools at moderate velocity. This is exemplified by the experiment from Figure 9, in which the DLR-LWR holding a knife moves along a desired trajectory in position or joint impedance-controlled mode, penetrating a silicone block. Figure 10 shows that with very low joint stiffness, the force and penetration depth increase much slower. For this particular trajectory, one presumably could prevent damaging the human skin. (Already contact forces of <80 N are enough to penetrate the human skin and cause further injury with a knives in case of stabbing [18]. However, with appropriate collision detection strategies, we confirmed in pig experiments that the DLR-LWR can avoid injuries with such sharp tools as knives up to certain velocity [19]. The additional compliance of the actuator will increase the time available to react and thus enables higher maximal velocities.)

Apart from these benefits, the problem of impacting in a pretensioned state or at very high joint velocities caused by striking out is of major focus for future research. This problem is especially important in the context discussed in the "Throwing" section, which shows a vast performance increase concerning link velocity by using the stored potential energy of the joint spring to further accelerate the link inertia.

These two examples illustrate the benefit of VSA design from the robot safety and performance point of view, and the next section will introduce the DLR-VSA design and present some experimental evidence of the performance increase and robot protection. Increasing human safety by VIA design is also a major issue, which will constitute the topic of a separate publication.

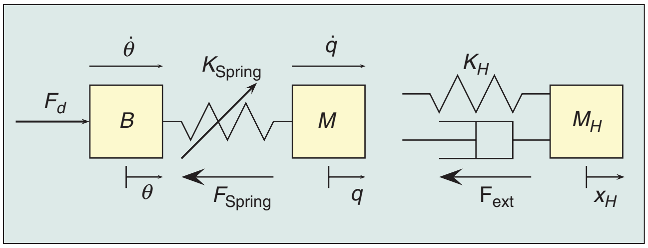

Figure 7. *1-DoF model of the impact between a VS robot and a human. The robot is modeled as a mass-spring-mass system, representing the motor mass, joint stiffness, and link mass. The human model is a Hunt-Crossley model harmonized with experimental crash test dummy data [11]. B, M were selected to be the reflected inertias in case of a typical stretched out collision configuration with the DLR-LWR-III, and K_{Spring} varied according to Figure 8.*

We are getting closer to the time when robots will finally leave the cages of industrial robotic workcells.

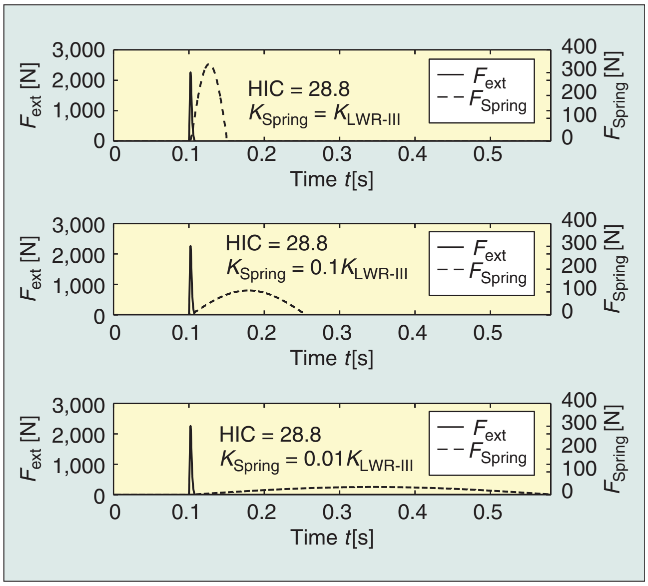

Figure 8. *Effect of joint stiffness reduction on impact force, HIC, and spring force during an impact with the human head at 2 m/s impact velocity. The spring force decreases in magnitude and increases in duration when lowering the spring stiffness. The joint stiffness K_{Spring} was chosen to be $K_{LWR-III}$, 0.1 $K_{LWR-III}$, and 0.01 $K_{LWR-III}$, i.e., 100%, 10%, and 1% of the reflected DLR-LWR-III joint stiffness.*

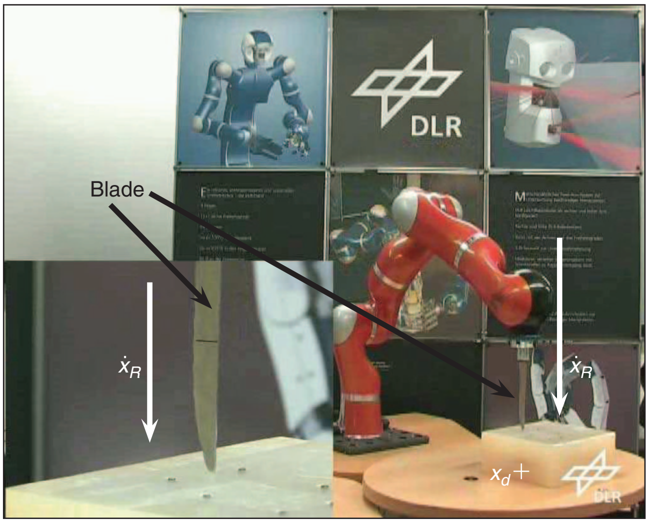

Figure 9. *The DLR-LWR-III equipped with a knife moves along a desired trajectory. The penetrated material is a silicone block. This experiment shows the benefit of intrinsic and controlled joint elasticity during impacts with sharp tools. The goal position x_d was approximately 7 cm inside the silicone block.*

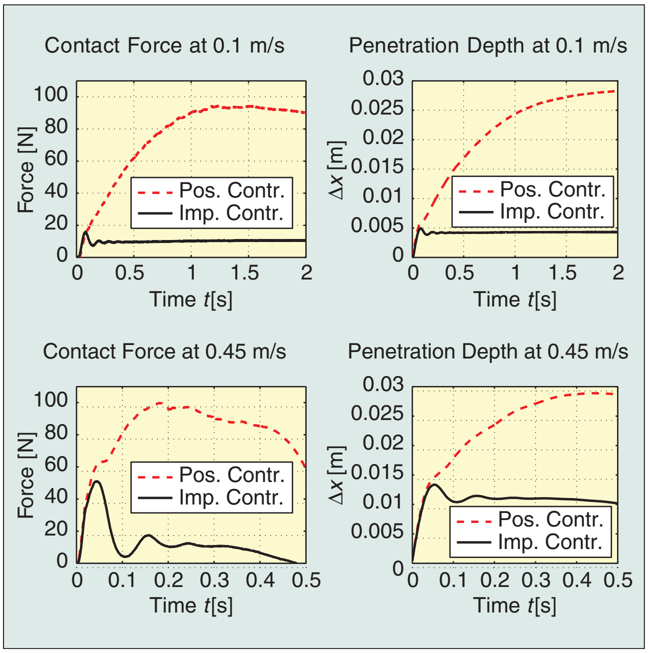

Figure 10. *Contact force and penetration depth for two different Cartesian velocities of 0.1 m/s and 0.45 m/s. Clearly, the benefit of the reduction of joint stiffness is apparent. The force level can be decreased even below levels that would potentially harm a human, whereas in position control, the force significantly exceeds this threshold. The goal position x_d was approximately 7 cm inside the silicone block.*

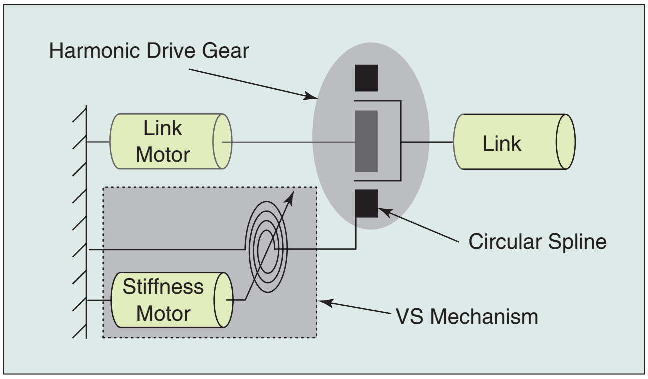

Figure 11. *Principle of joint mechanics. The circular spline of the harmonic drive gear is supported by the new mechanism.*

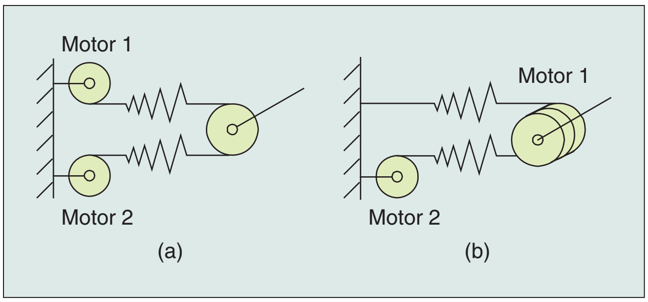

Figure 12. *VSA with nonlinear progressive springs in (a) antagonistic and (b) quasiantagonistic realization. In the later case, Motor 1 moves the joint, whereas Motor 2 is adjusting the stiffness.*

New Hardware Design Concepts

The simplest intrinsically compliant joint realization has a fixed spring behavior, usually with a constant or progressive stiffness characteristic. This results in a significant loss of link motion bandwidth and accuracy. To reduce this effect, the stiffness of the joint has to be adaptable to the desired task, requiring a second actuator. Several design approaches realizing robotic joints with variable mechanical stiffness are described in the literature [9], [13]–[16].

The biologically motivated concept of antagonistic actuation can already be found in some robotic systems [14], [20], [21]. In these realizations, two opposing actuators of similar size, each in combination with a series elastic element, were used. By running together in the same direction, the position is altered, and by moving in opposing direction, the link stiffness is adjusted [Figure 12(a)]. Unless nonbackdrivable gears are used, a high stiffness setting demands a constant torque of both actuators in opposing directions. This has some drawbacks in energy consumption. The approach in [22] aims at a reduction of these effects by motor cross coupling. As an advantage, the antagonistic principle provides in tendon driven joints an intrinsic robustness to kinematic errors. Furthermore, it is capable of completely distributing the power of both motors to stiffness changes or to the joint motion. The antagonistic principle is applied to the new tendon-controlled DLR hand.

Current work at DLR regarding robot arm joints is focused on a second option, in which one motor changes the link position and the other one the link stiffness almost independently [23]. This system leads to reduced dynamic losses and allows for stiffness adjustment independent from the link speed.

In our approach, the positioning motor is connected to the link via a harmonic drive gear. Mechanical compliance is introduced by a mechanism, which forms a flexible rotational support between the harmonic drive gear and the joint base (Figure 11). In case of a compliant deflection of the joint, the whole harmonic drive gear rotates relatively to the base, but the positioning motor is not moved. So, the link side inertia is altered only by the circular spline and some parts of the VS device. In contrast to that, the spring mechanism adds no inertia to the drive train between the positioning motor and the link. The link position is changed without moving the elasticity mechanism.

Two different mechanical compliant joint principles (patents pending) are derived from the previous considerations. A short overview of the principles is given in the following sections.

Quasiantagonistic Joint Mechanism

The elastic mechanism of the quasiantagonistic joint is derived from the antagonistic principle: two progressive elastic elements oppose each other, with a variable offset supporting the link with variable range of elastic motion (Figure 12).

The previously mentioned harmonic drive gear for link positioning is held in a bearing and has a cam bar attached to its normally fixed part (Figure 13). Two pairs of rocker arms act on different faces of this cam bar. External loads result in rotational displacement of the whole gear and force the rocker arms to spread against a linear spring, causing progressive restoring torque. The agonist rocker arms are fixed to the housing to save energy, whereas the antagonist part is positioned at a rotational offset by a stiffness actuator, which can change the stiffness very quickly and independent from the link speed [Figure 12(b)].

The shape of the cam faces can be designed to provide the desired restoring torque characteristic. Superposition of agonist and antagonist forces with different offsets results in variable stiffness. In the nominal range, it has (close to) linear behavior and gets progressive toward the ends of the range for joint protection.

It is clear that these human-friendly robots will look very different from today's industrial robots.

VS-Joint Mechanism

The concept of the VS joint as presented in [24] contains two motors of different size. The high-power motor changes the link position. The joint stiffness is adjusted by a much smaller and lighter motor, which changes the characteristic of the supporting mechanism (Figure 14). An unwound schematic of the principle is shown in Figure 15. A compliant link deflection results in a displacement of the cam disk and is counterbalanced by the roller pressed on it in axial direction by a spring. This generates a centering force resulting in the output torque of the link. To change the stiffness preset, the smaller motor moves the spring base axially to the cam disk and thus varies the spring force. The joint prototype can be equipped with different cam disks. The design of the cam disks specifies the torque/deflection characteristic of the joint. This permits an easy adaptation of the passive joint behavior to the desired application.

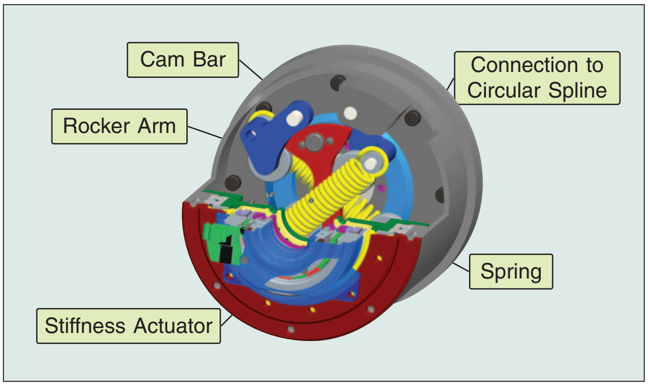

Figure 13. *Cross section of the quasiantagonistic joint design.*

Control of Variable Impedance Actuators

Regarding the control of the VIA, the literature mostly deals with the problem of adjusting stiffness and position of the actuator in a decoupled manner by controlling the position or the torque of the two motors of the joint [13], [15], [16]. Moreover, in case of VSA structures with many DoF and cable actuation, the decoupling of the tendon control is treated [25], [26].

Our approach to the control of the VSA arms is to extend the passivity-based control framework developed for the torque-controlled LWRs to the VSA case. Some particular aspects compared with the controllers from the "Compliance Control for Lightweight Arms" and "Impedance Control for Complex Kinematic Chains" sections are summarized.

- Because of the high compliance of the joint, a separate torque sensor is not required any more, and the torque can be well estimated based on the motor and link position [24].
- An active compliance control will be used only for stiffness components that cannot be realized by the mechanical springs. Examples are zero stiffness or the joint coupling stiffness needed by arbitrary Cartesian stiffness matrices [17].
- The joints have very low intrinsic damping. While this is useful for cyclic movements involving energy storage (e.g., for running), the damping of the arm for fast, precise positioning tasks has to be realized by control. This is a challenging task regarding the strong variation of the inertia and the stiffness. Figure 16 shows the performance of the positioning for a very low as well as for a very high stiffness preset of the VS joint.

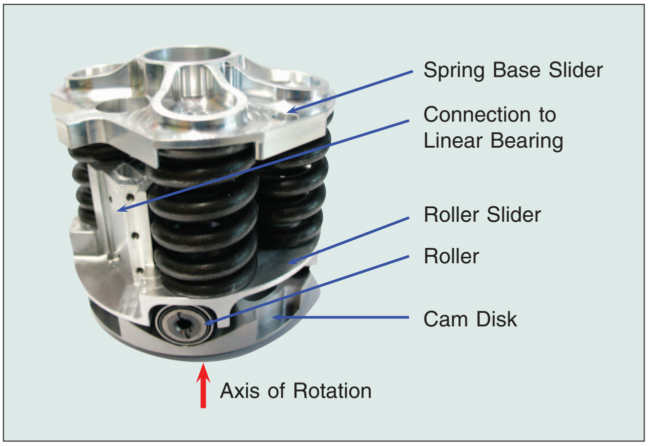

Figure 14. *VS-joint mechanism. The link axis is in the vertical direction. The cam disk rotates on a compliant link deflection.*

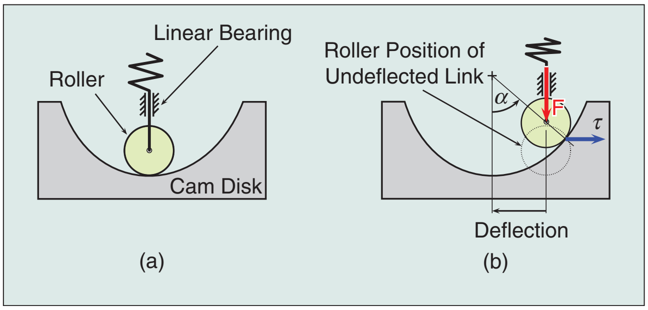

Figure 15. *Unwound schematic of the VS-joint principle in (a) centered and (b) deflected position. A deflection of the link results in a horizontal movement of the cam disk and a vertical displacement of the roller. The spring force generates a centering torque on the cam disk.*

- The pulling constraint of the tendons has to be fulfilled strictly. Decoupling algorithms will be used to ensure the realization of the passive joint stiffness, whereas the active joint stiffness can be varied over a large domain. Furthermore, a quasistatic effective joint stiffness can be given as a set point.

◆ Absolute accuracy of precise manipulation has to be realized using additional external sensing at the tip.

◆ The antagonistically tendon-driven joints of the hand (Figure 6) require the extension to handle nonlinear coupled joints based on the tendon coupling matrix.

◆ The pulling constraint of the tendons has to be fulfilled strictly. Decoupling algorithms will be used to ensure the realization of the passive joint stiffness, whereas the active joint stiffness can be varied over a large domain. Furthermore, a quasistatic effective joint stiffness can be given as a set point.

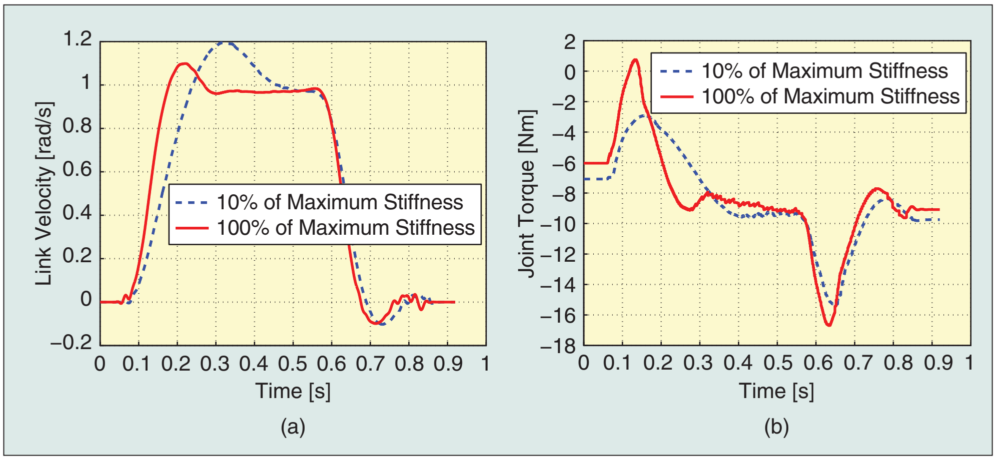

Figure 16. *Motion on a trajectory with rectangular velocity profile for small and maximal stiffness. (a) A critically damped velocity step response can be achieved independent from the stiffness and inertia value. (b) The effect of vibration damping is clearly observed in the torque signal, which contains only the acceleration peaks.*

Performance Validation

Along with the activity regarding the control of the joint, first experiments for validating the increase in performance were done.

Throwing

The application of throwing a ball is a good example to show the performance enhancement gained by the VS joint in terms of maximal velocity. For throwing a ball as far as possible, it has to be accelerated to the maximum achievable velocity and released at a 45° angle. The link velocity of a stiff link corresponds to the velocity of the driving motor. In a flexible joint, the potential energy stored in the system can be used to accelerate the link relatively to the driving motor. Additional energy can be inserted by the stiffness adjuster of the VS joint to gain an even faster motion.

A lacrosse stick head was mounted on the top of the link lever for the throwing tests. The ball is a 64-g rubber ball for school lacrosse. The distance between the link axis and the center of the ball when the ball leaves the lever is approximately 0.78 m.

A simple strikeout trajectory is used to gain high link velocity (Figure 17). It uses the resonance effect of the mass-spring system to maximize joint velocity. With the measured maximum link velocity of 572°/s, the throwing distance was approximately 6 m, corresponding well to the calculated distance of 6.18 m. The theoretical throwing distance with an inelastic link of the same setup with the same maximum motor velocity of 216°/s is 0.88 m, also confirmed experimentally. A speed gain of 265% for the link velocity between rigid and compliant joint was achieved in the test.

Compared with a human, the throwing range of the VS joint seems small, but one has to keep in mind that this was done by a single joint, whereas a human uses several DoF including the hip joints. A series arrangement of joints in a robot arm enlarges the achievable distance.

Stiffness Adjustment

A similar increase of velocity could also be realized by a series elastic actuator without adjustable stiffness. Figure 16 shows the advantage of the VSA design. Fast positioning can be

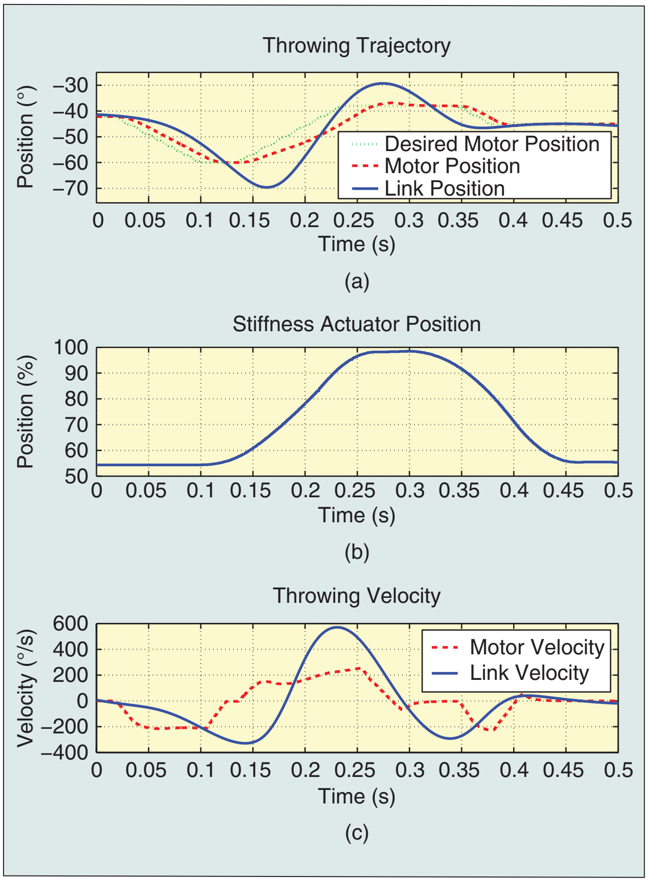

Figure 17. *(a) Throwing trajectory. (b) Stiffness motor position. (c) Joint velocities.*

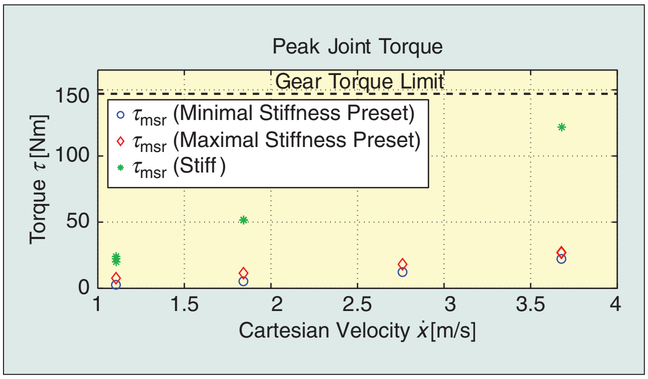

Figure 18. *Peak joint torque during impacts with the VS joint. The impact velocity ranges up to the maximum velocity of the KR500/Robocoaster on which the joint was mounted for the experiment.*

achieved by increasing the stiffness. On the other hand, lowering the stiffness can be used in certain situations for protecting the robot from external loads, as described in the "Protecting the Robot Joint and the Human by Variable Joint Stiffness" section, and validated by the following experiment. (An article with detailed discussion of the load reduction of the joint is currently in preparation.)

Experimental Validation of Joint Overload Protection

To validate the results from the "Protecting the Robot Joint and the Human by Variable Joint Stiffness" section, the impact of the joint at a predefined velocity with a test object was evaluated. Two stiffness setups are realized via the passively compliant VS joint. The most compliant as well as the stiffest configuration were chosen. In a third setup, a mechanical shortcut is inserted into the test bed instead of the VS joint mechanism such that a much stiffer joint is obtained (in the range of the DLR-LWR-III joint elasticity).

Both increasing impact speed and increasing joint stiffness result in higher peak joint torques as visualized in Figure 18. The maximum peak torque limit of the joint gear is almost reached with the stiff joint at an impact velocity of approximately 3.7 m/s, whereas the compliant VS joint is still far in the safe torque region.

Conclusions

In this article, we gave an overview on the DLR activities related to two approaches for the realization of soft robotics: actively torque-controlled LWRs and VSA. On the basis of our experience with torque-controlled robots, we presented an analysis on expected advantages and also disadvantages of VSA actuators. Furthermore, two VSA joint designs motivated by this analysis were presented.

Torque-controlled robots currently represent a technology mature enough for the market, but we believe that impressive research progress can be expected in the area of VSA-actuated robots in the next decade.

Keywords

Soft robotics, lightweight robot, joint torque control, variable compliance actuators.

References

[1] A. Albu-Schäffer, C. Ott, and G. Hirzinger, "A unified passivity based control framework for position, torque and impedance control of flexible joint robots," *Int. J. Robot. Res.*, vol. 26, no. 1, pp. 23–39, 2007.

[2] C. Ott, A. Albu-Schäffer, A. Kugi, and G. Hirzinger, "On the passivity based impedance control of flexible joint robots," *IEEE Trans. Robot. Automat.*, vol. 24, no. 2, pp. 416–429, 2008.

[3] A. Albu-Schäffer, C. Ott, and G. Hirzinger, "A passivity based cartesian impedance controller for flexible joint robots, Part II: Full state feedback, impedance design and experiments," in *Proc. IEEE Int. Conf. Robotics and Automation*, 2004, pp. 2666–2673.

[4] E. Fasse and J. Broenink, "A spatial impedance controller for robotic manipulation.," *IEEE Trans. Robot. Automat.*, vol. 13, no. 4, pp. 546–556, 1997.

[5] F. Caccavale, C. Natale, B. Siciliano, and L. Villani, "Six-dof impedance control based on angle/axis representations," *IEEE Trans. Robot. Automat.*, vol. 15, no. 2, pp. 289–299, 1999.

[6] S. Stramigioli and V. Duindam, "Variable spatial springs for robot control applications," in *Proc. IEEE/RSJ Int. Conf. Intelligent Robots and Systems*, 2001, pp. 1906–1911.

[7] T. Wimböck, Ch. Ott, and G. Hirzinger, "Passivity-based object-level impedance control for a multifingered hand," in *Proc. IEEE/RSJ Int. Conf. Intelligent Robots and Systems*, 2006, pp. 4621–4627.

[8] S. Stramigioli, *Modeling and IPC Control of Interactive Mechanical Systems: A Coordinate-Free Approach*, vol. 266, (Lecture Notes in Control and Information Sciences Series). New York: Springer-Verlag, 2001.

[9] T. Morita, H. Iwata, and S. Sugano, "Development of human symbiotic robot: Wendy," in *Proc. IEEE Int. Conf. Robotics and Automation*, 1999, pp. 3183–3188.

[10] S. Haddadin, T. Laue, U. Frese, and G. Hirzinger, "Foul 2050: Thoughts on physical interaction in human-robot soccer," in *Proc. IEEE/RSJ Int. Conf. Intelligent Robots and Systems*, San Diego, 2007, pp. 3243–3250.

[11] S. Haddadin, A. Albu-Schäffer, and G. Hirzinger, "Safety evaluation of physical human-robot interaction via crash-testing," in *Proc. Robotics: Science and Systems Conf. (RSS2007)*, Atlanta. [Online]. Available: http://www.roboticsproceedings.org

[12] I. P. Herman, *Physics of the Human Body.* New York: Springer-Verlag, 2007.

[13] A. Bicchi and G. Tonietti, "Fast and soft arm tactics: Dealing with the safety-performance trade-off in robot arms design and control," *IEEE Robot. Automat. Mag.*, vol. 11, no. 2, pp. 22–33, 2004.

[14] S. A. Migliore, E. A. Brown, and S. P. DeWeerth, "Biologically inspired joint stiffness control," in *Proc. IEEE Int. Conf. Robotics and Automation*, Barcelona, Spain, 2005, pp. 4519–4524.

[15] G. Palli, C. Melchiorri, T. Wimboeck, M. Grebenstein, and G. Hirzinger, "Feedback linearization and simultaneous stiffness-position control of robots with antagonistic actuated joints," in *Proc. IEEE Int. Conf. Robotics and Automation (ICRA2007)*, Rome, Italy, 2007, pp. 2928–2933.

[16] B. Vanderborght, B. Verrelst, R. V. Ham, M. V. Damme, D. Lefeber, B. M. Y. Duran, and P. Beyl, "Exploiting natural dynamics to reduce energy consumption by controlling the compliance of soft actuators," *Int. J. Robot. Res.*, vol. 25, no. 4, pp. 343–358, 2006.

[17] A. Albu-Schäffer, M. Fischer, G. Schreiber, F. Schoeppe, and G. Hirzinger, "Soft robotics: What cartesian stiffness can we obtain with passively compliant, uncoupled joints?" in *Proc. IEEE Int. Conf. Intelligent Robotic Systems*, 2004, pp. 3295–3301.

[18] S. Haddadin, A. Albu-Schäffer, and G. Hirzinger, "Safe physical human-robot interaction: Measurements, analysis and new insights," in *Proc. Int. Symp. Robotics Research*, Hiroshima, Japan, 2007.

[19] S. Haddadin, A. Albu-Schäffer, A. De Luca, and G. Hirzinger, "Evaluation of collision detection and reaction for a human-friendly robot on biological tissues," in *Proc. IARP Int. Workshop on Technical Challenges and for Dependable Robots in Human environments*, Pasadena, 2008. [Online]. Available: http://www.robotic.de/fileadmin/robotic/haddadin/haddadin_et_al_iarp2008.pdf

[20] K. Koganezawa, "Mechanical stiffness control for antagonistically driven joints," in *Proc. IEEE/RSJ Int. Conf. Intelligent Robots and Systems*, Aug. 2005, pp. 2512–2519.
[21] C. English and D. Russell, "Implementation of variable joint stiffness through antagonistic actuation using rolamite springs," *Mech. Mach. Theory*, vol. 34, no. 1, pp. 27–40, 1999.
[22] G. Tonietti, "Variable impedance actuation," Ph.D. dissertation, University of Pisa, 2005.
[23] T. Morita and S. Sugano, "Development and evaluation of seven-d.o.f. mia arm," in *Proc. 1997 IEEE Int. Conf. Robotics and Automation*, Sept. 1997, pp. 462–467.
[24] S. Wolf and G. Hirzinger, "A new variable stiffness design: Matching requirements of the next robot generation," in *Proc. IEEE Int. Conf. Robotics and Automation*, Pasadena, CA, 2008, pp. 1741–1746.
[25] H. Kobayashi and R. Ozawa, "Adaptive neural network control of tendon-driven mechanisms with elastic tendons," *Automatica*, vol. 39, pp. 1509–1519, 2003.
[26] K. Tahara, Z.-W. Luo, R. Ozawa, J.-H. Bae, and S. Arimoto, "Bio-mimetic study on pinching motions of a dual-finger model with synergistic actuation of antagonist muscles," in *Proc. IEEE Int. Conf. Robotics and Automation*, 2006, pp. 994–999.
[27] S. Haddadin, A. Albu-Sch, A. De Luca, and G. Hirzinger, "Collision detection and reaction: A contribution to safe physical human-robot interaction," in *Proc. IEEE/RSJ Int. Conf. on Intelligent Robots and Systems*, Nice, France, 2008.

Alin Albu-Schäffer received the Dip.-Ing. degree in electrical engineering from the Technical University of Timisoara, Romania in 1993 and the Ph.D. degree in control systems from the Technical University of Munich (TUM), Germany, in 2002. Since 1995, he has been working with the German Aerospace Center (DLR), Institute of Robotics and Mechatronics, Wessling, Germany, where he is currently coordinating the control and advanced manipulation activities. His current research interests include robot modeling and control, nonlinear control, flexible joint robots, impedance and force control, physical human-robot interaction, and variable impedance actuation.

Oliver Eiberger received his Dipl.-Ing. degree in mechanical engineering from TUM in 2000 and joined DLR in the same year. He is working on DLR Robot arm designs and the quasiantagonistic joint concept.

Markus Grebenstein received his diploma in mechanical engineering in 1996 from TUM. Since 1996, he has been with the DLR, Institute of Robotics and Mechatronics. Since May 2000, he has been leading the mechanical design group. His main research focus is the design of anthropomorphic multifingered robot hands and the design of lightweight robot joints. He published 24 papers on these topics, holds more than eight patents, and has about five patents pending.

Sami Haddadin received his Dipl.-Ing. degree in electrical engineering in 2006 from TUM and holds an honors degree in technology management from TUM and the Ludwig Maximilian University in Munich. He currently works at the DLR as a research engineer. His main research topics are physical human-robot interaction, robot control, and safety and dependability in robotics.

Christian Ott received his Dipl.-Ing. degree in mechatronics from the Johannes Kepler University (JKU), Linz, Austria, in 2001, and the Dr.-Ing. degree in control engineering from Saarland University, Saarbrücken, Germany, in 2005. From March 2001 to April 2007, he was with the DLR, Institute of Robotics and Mechatronics, Wessling, Germany. Since May 2007, he has been a project assistant professor in the Department of Mechano-Informatics, University of Tokyo, Japan. His current research interests include nonlinear control of robotic systems, flexible joint robots, impedance control, and two-armed humanoid manipulation.

Thomas Wimböck studied electrical engineering at the Rensslaer Polytechnic Institute, Troy, and at the Ecole Polytechique Fédérale de Lausanne, Switzerland. He received his B.Sc. and M.Sc. (in 2004) degrees in electrical engineering from TUM. In 2004, he joined the DLR, Institute of Robotics and Mechatronics, as a Ph.D. student. His main research interests include nonlinear control, dexterous robot hands, impedance control, VS control, two-handed (humanoid) manipulation, and kinematic redundancy.

Sebastian Wolf received his Dipl.-Ing. degree in mechanical engineering in 2004 from TUM, Germany. He joined the Institute fur Feingeratebau und Mikrotechnik at TUM, Germany, as a research associate in 2004. Since 2005, he has been a research engineer at the DLR, Institute of Robotics and Mechatronics. His main research interest is in VS actuation.

Gerd Hirzinger received the Dipl.-Ing. and Ph.D. degrees from TUM, Germany, in 1969 and 1974, respectively. Since 1992, he has been the director at the DLR, Institute of Robotics and Mechatronics, Wessling, Germany. In 1991, he received a joint professorship from TUM and in 2003, an honorary professorship at the Harbin Institute of Technology, China. He was a prime investigator of the first remote control space robot ROTEX, which flew onboard the shuttle Columbia in April 1993. He is the recipient of numerous national and international awards, including the Joseph-Engelberger-Award for achievements in robotic science in 1994, the Leibniz-Award, in 1995, the Japan Robotics Association (JARA) Award, the Karl-Heinz-Beckurts-Award in 1996, and the IEEE Fellow Award in 1997. In 2004, he received the order of merit of the Federal Republic of Germany and became a member of the Wall of Fame of the Heinz Nixdorf Computer Museum. He is also the recipient of the IEEE Pioneer Award of the Robotics and Automation Society, the 2005 Honorary Citizenship of Budapest Tech, and the IEEE Field Award Robotics and Automation in 2007.

Address for Correspondence: Alin Albu-Schäffer, DLR-German Aerospace Center, P.O. Box 1116, 82230 Wessling, Germany. E-mail: alin.albu-schaeffer@dlr.de.